International Journal of Refrigeration 134 (2022) 265–277

Contents lists available at ScienceDirect

International Journal of Refrigeration

journal homepage: www.elsevier.com/locate/ijrefrig

Experimental investigation of dedicated desiccant wheel outdoor air cooling systems for nearly zero energy buildings

Étude expérimentale de systèmes de refroidissement de l'air extérieur par roue déshydratante pour les bâtiments à énergie quasi nulle

Liu Chen *, Yujie Chu, Wenjie Deng

Energy School, Xi'an University of Science and Technology, Yanta Road Xi'an 710054, P.R. China

ARTICLE INFO

Keywords:
Nearly zero energy building
Desiccant wheel
Heat pipe heat exchanger
Dedicated outdoor air system

Mots clés:
Bâtiment à énergie quasi nulle
Roue déshydratante
Échangeur de chaleur à caloduc
Système à air extérieur dédié

ABSTRACT

In high-temperature and high-humidity environments, a large amount of energy is consumed to cool and dehumidify outdoor air by dedicated outdoor air systems in nearly zero energy buildings. Desiccant wheels have the advantages of large moisture removal capacities and continuous regeneration. However, the application of desiccant wheels in nearly zero energy buildings is limited by their large regeneration heat capacity and high temperature after dehumidification. A dedicated desiccant wheel outdoor air cooling system is thus proposed. An experimental setup is built and used to test the performances of three modes for dedicated desiccant wheel outdoor air cooling systems. The results show that mode I (wet membrane humidifier downstream evaporation section of heat pipe heat exchanger) has a higher performance coefficient and higher exergy efficiency compared to other modes. The thermodynamic and exergy performances of the proposed mode I system are determined. The results show that the thermodynamic coefficient decreases from 1.3 to 0.52 and the exergy efficiency decreases from 0.76 to 0.18 when the regeneration temperature increases from 60°C to 110°C.

1. Introduction

Nearly zero energy buildings (nZEBs), which are a redevelopment of energy-saving buildings, symbolize developing trends in future buildings with low levels of energy consumption and high levels of indoor comfort characteristics (Shu et al., 2020, Lopez-Ochoa et al., 2019, Li et al., 2021, Papadopoulos et al., 2019). nZEBs improve energy efficiency through various energy-saving methods by using renewable energy to meet energy demand and achieve the goal of not consuming traditional energy to the greatest extent possible. Air conditioning systems contribute the most to the energy consumption of building operations (Huang et al., 2020, Jahani et al., 2020). A large amount of energy is consumed in dedicated outdoor air systems (DOASs) to handle fresh air because of the significant enthalpy difference between fresh air and indoor air (Liu et al., 2018). Therefore, investigating dedicated outdoor air cooling systems is of great significance for nZEBs.

Traditional DOASs, which use a vapour compression refrigeration cycle, always couple refrigeration and dehumidification (Chuah and Yang, 2020, Yang et al., 2020, Cheon et al., 2021). Although this method is easy to achieve, the air must be cooled below the dew point temperature for dehumidification. nZEBs have a low ratio of sensible heat to total heat in hot humid climates (Tian et al., 2021). Traditional DOASs in a hot humid climate require high levels of energy consumption to satisfy the requirements for cooling and dehumidification. In addition, the high electricity demand and large CFC emissions from traditional DOASs exacerbate global warming, which is not conducive to the realization of carbon neutrality goals (Jani et al., 2018, Tang et al., 2021).

Compared with the vapour compression refrigeration cycle, the desiccant wheel air conditioning system has been studied and attracted considerable attention due to its remarkable energy saving potential and environmental benefits (Jani et al., 2016, Asadi et al., 2020, Ukai et al., 2018). Desiccant regeneration heat accounts for a large share of the energy consumption, and the common regeneration heat sources are solar energy, heat pumps, microwaves, waste heat and electric heaters (Tu and Hwang, 2018, Kubota et al., 2013). Solar energy, as a nonpolluting energy source, is an ideal regeneration heat source as a kind of renewable energy. Chaudhary et al. (Chaudhary et al., 2018) combined

* Corresponding author.
E-mail address: chenliu@xust.edu.cn (L. Chen).

https://doi.org/10.1016/j.ijrefrig.2021.11.016
Received 5 July 2021; Received in revised form 9 November 2021; Accepted 24 November 2021
Available online 28 November 2021

Nomenclature

c	cost per exergy rate, \$ kW^{-1}
$\dot{C}$	Exergy cost rate, \$/h
C_p	specific heat capacity, kJ $kg^{-1}\bullet K^{-1}$
CRF	capital recovery factor
d	discount rate
D_{sys}	moisture removal efficiency
$\dot{E}$	exergy rate, kW
e	specific exergy, kJ kg^{-1}
H_V	water latent heat of vaporization, kJ kg^{-1}
i	interest rate
IC	investment cost, \$
LCC	life cycle cost, \$
$\dot{M}$	mass flow rate, kg s^{-1}
MRC	moisture removal capacity, g s^{-1}
N	operational hours in a year, h
n	system life time, year
OC	operation cost, \$
P	vapor partial pressure, Pa
PBP	payback period, year
R	ideal gas constant, kJ $kg^{-1}\bullet K^{-1}$
RH	relative humidity, %
RHC	regeneration heat capacity, kW
SHC	sensible heat capacity, kW
SHE	sensible heat efficiency
T	temperature, K
t	temperature, ℃
$TCOP$	thermodynamic coefficient
$\dot{Q}$	heat transfer rate, kW
$\dot{W}$	work rate, kW
y	destruction exergy ratio
Z	capital cost, \$
$\dot{Z}$	capital cost rate, \$/h
Greek symbols	
η	exergy efficiency
ϕ	maintenance factor
ω	humidity ratio, g kg^{-1}
Subscript	
a	*air*
$conv$	conventional system
d	destruction
e	exit
f	fuel
i	inlet
k	Kth component
p	production
pro	process air
$prop$	proposed system
q	heat
r	reference condition
reg	regeneration air
s	saturated air
sys	system
v	*water vapor*
W	water
w	work
Abbreviations	
AH	air heater
DOAS	dedicated outdoor air system
DW	desiccant wheel
DWDOAS	dedicated desiccant wheel outdoor air cooling systems
EH	electric heater
HP	heat pipe heat exchanger
nZEB	nearly zero energy building
MOF	metal-organic framework material
WMH	wet membrane humidifier

a solar system, desiccant wheel and a Maisotsenko cycle (MC)-based evaluative cooling system. The efficiency of the collector was improved, and the COP of the system increased from 0.65 to 1.17 by coupling the evacuated tubular collectors with a flat plate collector. Heidari et al. (Heidari et al., 2019) combined a solar system with desiccant-based evaporative cooling to maintain indoor relative humidity at approximately 60% during hot summers. Compared with a traditional system, the energy consumption of the system was reduced by 60%. Chen and Tan (Chen and Tan, 2020) proposed a solar desiccant wheel air conditioning system using high-temperature chilled water, which was applied for high and moderately humid conditions. The COP of the system reached 2.2 by using a solar water heating system to reduce the regeneration energy consumption of the desiccant wheel.

However, renewable energy, including solar heat and heat pumps, cannot precisely match the latent load of a building due to the influence of seasons, weather and other factors. Auxiliary heat sources are needed, which greatly reduce the energy efficiency of the system for meeting the dehumidification demand for a nZEB. Therefore, the energy consumption of an auxiliary heat source should be reduced when the system is applied to a nZEB. A heat pipe heat exchanger (HP), which is an efficient phase change heat transfer equipment, can transfer large amounts of heat at a small temperature difference with a compact size (Yue et al., 2019, Milani et al., 2016, Anand et al., 2020, Qu et al., 2018). Wang et al. (Wang et al., 2016) proposed an air conditioning system that used an HP to realize heat recovery. Compared with the common heat recovery air conditioning system, energy can be reduced by 2.5% in the summer and 22.1% in the winter. The heat recovery efficiency can reach 60.2%. Monirimanesh et al. (Monirimanesh et al., 2016) applied HP to air conditioning systems and found that up to 40% of the heat was recovered.

The sensible heat load of the desiccant wheel air conditioning system needs a cooling facility, commonly, a water-cooled-type cooler, heat pump evaporator and evaporative cooler. Chen et al. (Chen et al., 2018) proposed a precooling desiccant wheel air conditioning system that used a two-stage water-cooled type cooler to reduce system temperature rise. The dehumidification efficiency and enthalpy efficiency were significantly increased in comparison to those of one-stage systems. Martinez et al. (Martinez et al., 2018) used TRNSYS to simulate and compare a desiccant wheel air conditioning system using a heat pump and an indirect evaporative cooler. Their research showed that the desiccant wheel air conditioning system using an indirect evaporative cooler consumes less primary energy. This energy reduction will inevitably lead to energy wastage when using water-cooled coolers, evaporators and indirect evaporative coolers, which have a strong ability to bear an excessive sensible heat load in a low sensible heat nZEB. Some researchers have conducted research on direct evaporative coolers as green and sustainable cooling equipment. They have shown that the cooling efficiency is related to the packing materials, packing thickness, air velocity, air temperature, air humidity and other factors (He et al., 2014, Malli et al., 2011, Kabeel and Bassuoni, 2017). Chiesa et al. (Chiesa et al., 2019) studied the possibility of applying direct evaporative coolers to increase thermal comfort in 60 different regions of the Mediterranean through simulations. The results showed that the thermal comfort performance of direct evaporative coolers mainly depends on the sensible load of buildings. In the Mediterranean, direct evaporative coolers can achieve the best operation as a low-energy system.

As described above, most of the previous studies have focused on the performance of DOASs for general buildings, while very few studies have been performed for nZEBs. DOASs for nZEBs are completely different from DOASs for general buildings because of the differences in heat load performance and energy saving requirements. Therefore, the development of high-performance and energy-saving DOASs is important, especially in hot and humid climates. To solve the problem of the unsuitability of traditional DOASs for nZEBs, this study aims to develop dedicated desiccant wheel outdoor air cooling systems (DWDOAS), which combine a desiccant wheel, a heat pipe heat exchanger and a wet membrane humidifier. The heat pipe heat exchanger can transfer large amounts of the adsorption heat released from the desiccant wheel to the regeneration heat, thereby reducing the regeneration energy consumption of the DWDOAS. A wet membrane humidifier with low energy consumption and compactness is applied as a direct evaporative cooler to achieve a sensible heat load. Three modes of DWDOAS are proposed,

and the thermodynamic and exergy performance of the DWDOAS under the different modes are studied experimentally to obtain the optimal DWDOAS mode. For the optimal DWDOAS mode, the influence of the main parameters on system thermodynamics and exergy performance is studied experimentally, and the economic performance of the proposed system is carried out and compared to those of a conventional air conditioning system.

2. Method

2.1. Working principle

A schematic diagram of a DWDOAS is shown in Fig. 1. It mainly consists of six components: the DW, HP, WMH, process fan, regenerative fan, and air heater. The DW performs the process and regeneration at alternating intervals. The thermal energy from solar energy is available to heat the regeneration air of the desiccant in the DW, assisted by auxiliary electric heater when solar energy is insufficient. The HP is composed of a group of heat pipes (two-phase closed thermosyphon), and the central part is partitioned to divide the HP into an evaporator section and a condenser section. Two-phase closed thermosyphons are simple to fabricate. The core of the WMH is a wet film material composed of polymer composites. Under the effect of gravity, water sent to the top of the humidifier percolates down along the surface of the wet membrane to form an even water membrane on the surface of the wet membrane and then cools and humidifies the hot and dry air.

Dedicated desiccant wheel outdoor air cooling systems are designed to have two flow paths: the process side and the regeneration side. The process side for outdoor air processing meets the temperature and humidity requirements of the buildings. The regeneration side is responsible for generating heat energy and separating the moisture absorbed by the DW. The critical design questions of a DWDOAS would be to decide on the placement of the WMH, either downstream of the HP evaporation section to cool the outdoor air or upstream of the HP condensation section to precool the regenerative air, which can enhance the heat transfer of the HP. Based on the above situation, three DWDOAS modes are proposed, as shown in Fig. 1.

As shown in Fig. 1, in mode I, valves CV1 and CV4 are closed, and valves CV2 and CV3 are open to place WMH 1 downstream of the HP evaporation section. Outdoor air passes through the process side of the DW, water vapour is absorbed, and adsorption heat is released. State A is heated and dehumidified to state B, state B is cooled to state C by the evaporator section of the HP, and state C is cooled to state C' by the WMH 1. Then, the supply air (state S) is supplied to the building's interior by the process fan. The regeneration inlet air (state R) from the building is heated to state D through the condenser section of the HP and then heated to state E by a solar heater. State E is high-temperature air, which desorbs the water in the adsorption material through the regeneration side of the DW, and then this humid air (state F) is exhausted by the regeneration fan.

As shown in Fig. 1, in mode II, valves CV2 and CV3 are closed, and valves CV1 and CV4 are open to place the WMH 2 upstream of the HP condensation section. After passing through the process side of the DW, the outdoor air enters the HP evaporation section and is directly sent into the room through the process fan. State R is precooled at the regeneration inlet to point R' by WMH 2, heated to point D through the HP condensation section, heated to the rated regeneration temperature through solar energy, and finally discharged through the regeneration fan on the DW regeneration side.

As shown in Fig. 1, in mode III, valves CV1 and CV2 are closed, and valves CV3 and CV4 are open to place WMH 1 downstream of the HP evaporation section and WMH 2 upstream of the HP condensation section. Outdoor air is sent into the building after passing through the DW process side, HP evaporation section and WMH. The regeneration air then enters the HP evaporation section after precooling via WMH and is then heated to the rated regeneration temperature via solar energy. Finally, it passes through the DW regeneration side and is exhausted.

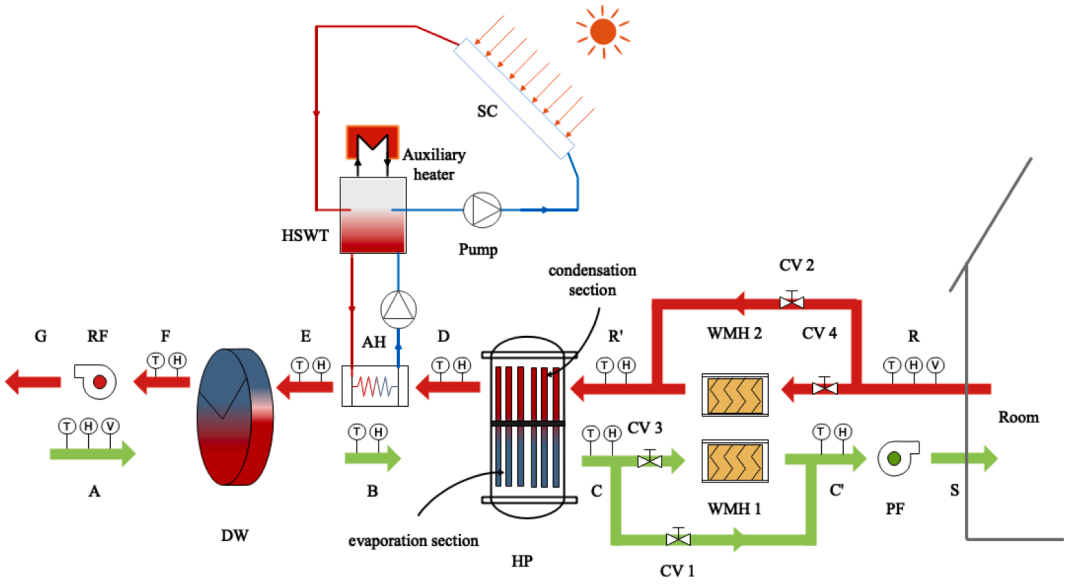

Fig. 1. Schematic diagram of the DWDOAS.

2.2. Experimental setup

A set of experimental setups consisting of an air-preconditioning unit, a desiccant wheel, a heat pipe heat exchanger, and a wet membrane humidifier and data acquisition system based on the above principles was established and is shown in Fig. 2. In the experiment, an electric heater was used to replace the solar heater in Fig. 1. The air-preconditioning unit was provided by Nanjing TICA Air Conditioning Co., Ltd., China, the characteristics of which are shown in Table 1. The air-preconditioning unit passed the process air through the direct expansion cooling unit, an electrode humidification unit, an electric heating unit and a fan to meet the outdoor air requirements of the experiment. The DW selected was a USD-10D model produced by Wuxi Lianzhong Humidifier & Energy Saving Equipment Co., Ltd., China, the characteristics of which are shown in Table 2. The performance parameter of the HP was determined by design and calculation. The HP was provided by the manufacturer of the HP, as specified. The HP was manufactured by Beijing Dtdx Co., Ltd., China, the structural parameters of which are shown in Table 3. The selection of the WMH was performed according to the required air volume. The WMH used was a YSMF-1.5 model produced by Beijing Yushilong Technology Development Co., Ltd., China, the parameters of which are shown in Table 4.

2.3. Experimental conditions

Through the above experimental device, the performance of the DWDOAS was studied. In the experimental study, the regeneration inlet air parameters were kept constant. One of the operating parameters of the DWDOAS was varied, while all other operating parameters were kept constant (base value). Table 5 shows the experimental conditions.

2.4. Exergy analysis

Exergy analysis was conducted based on steady-state conditions. Based on the exergy rate balance, the exergy rate balance for the kth component of the DWDOAS is as follows:

$$\sum_e (\dot{M}_e e_e)_k + \dot{W}_k = \left[1 - \left(\frac{T_r}{T_k}\right)\right]\dot{Q}_k + \sum_i (\dot{M}_i e_i)_k \tag{1}$$

or

$$\sum_e \dot{E}_{e,k} + \dot{W}_k = \dot{E}_{q,k} + \sum_i \dot{E}_{i,k} \tag{2}$$

Table 1
Characteristics of the air-preconditioning unit.

Parameters	Capacity
Nominal refrigeration capacity	26.0 kW
Nominal heating capacity	29.0 kW
Nominal humidifying capacity	0.01 kg/s

Table 2
Characteristics of the DW.

Parameters	Capacity
Nominal capacity	0.002625 kg/s
Nominal air flow on process side	0.42 m^3/s
Desiccant material	Silica gel
Diameter	550 mm
Thickness	200 mm
Regeneration angle	90°
Channel shape	Honeycomb
Rotation speed	12 r/h

Table 3
Specifications of the HP.

Parameters	Capacity
Working fluid of the heat pipe	Nitrogen
Shell material	Aluminium alloy
Nominal air flow	0.28 m^3/s
Heat exchange area	53.7 m^2
Single heat pipe length	1050 mm
Base tube size	24 mm
Fin size (height * spacing * thickness)	10*2.1*0.4 (mm*mm*mm)
Shape size	1080*410*540 (mm*mm*mm)
Inter-tube distances	45 mm
Number of heat pipes	44
Total number of rows	8
Dimension of heat exchanger	1080*410*540 (mm*mm*mm)

The exergy of the air, which consists of 1 kg of dry air and ω kg of water vapour, was calculated using the following equation (Zhang et al., 2015):

$$e_a = (C_{p.a} + \omega C_{p.v})T_r\left(\frac{T}{T_r} - 1 - ln\frac{T}{T_r}\right) + R_a T_r\left[(1+1.608\omega)ln\frac{(1+1.608\omega_r)}{(1+1.608\omega)} + (1.608\omega)ln\frac{\omega}{\omega_r}\right] \tag{3}$$

The exergy of the water was calculated using the following equation

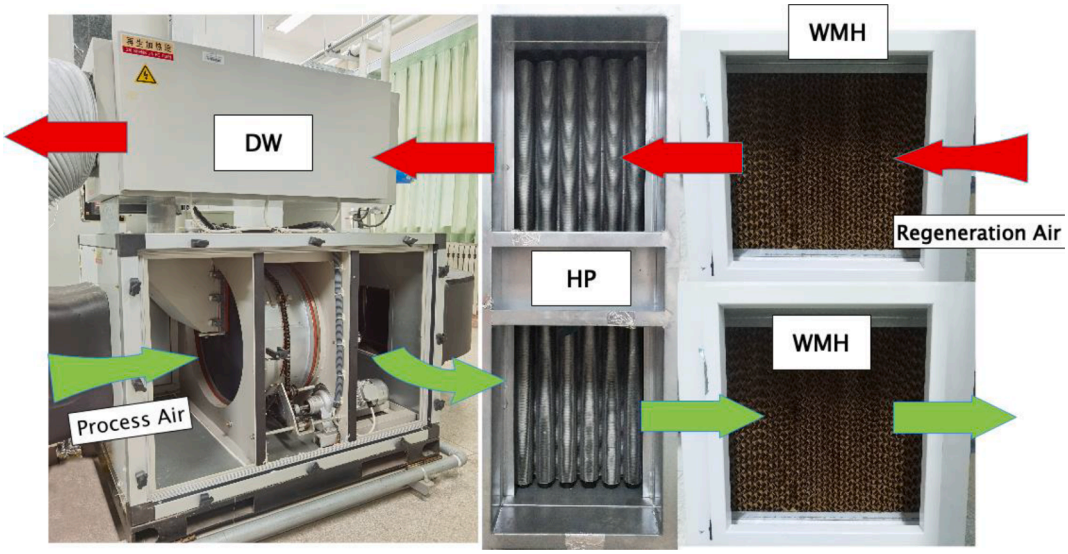

Fig. 2. Photograph of the experimental setup of the DWDOAS.

Table 4
Characteristics of the WMH.

Parameters	Capacity
Nominal humidification	0.00125 kg s^{-1}
Nominal air volume	0.42 m^3 s^{-1}
Packing material	Celdek
Dimensions	600*500*500 (mm*mm*mm)

Table 5
Experimental conditions.

Parameters	Range value	Base value
Process air inlet temperature, T_A (℃)	28~38	32
Process air inlet humidity ratio, ω_A (g kg^{-1})	14~22	18
Process air mass flow rate, M_{pro} (m^3 s^{-1})	0.12~0.32	0.2
Regeneration air inlet air temperature, T_R (℃)	-	25°C
Regeneration air inlet air humidity ratio, ω_R (g kg^{-1})	-	8.8 g/kg
Regeneration air mass flow rate, M_{reg} (m^3 s^{-1})	-	0.15 m^3/s
Regeneration temperature, T_{Ah} (℃)	60~110	80

(Wang and Li, 2011):

$$e_W = c_{p,W}(T - T_r) - T_r c_{p,W} ln\frac{T}{T_r} + T_r R_v ln\frac{P_{v,s}}{P_{v,r}} - H_V\left(1 - \frac{T}{T_r}\right) \quad (4)$$

The reference temperature and humidity ratio of the air were set to 35°C and 36.55 g kg^{-1}, respectively. The reference temperature of the water was set to 15°C.

The productive purpose of a process unit or component measured in terms of exergy is called the production. The exergy flow that is consumed to create the production is called fuel Valero et al., 2006). Based on Eqs. (1) and ((2), the fuel exergy rate ($\dot{E}_f$), production exergy rate ($\dot{E}_p$) and destruction exergy ($\dot{E}_d$) of each component in the proposed DWDOAS system with mode I are presented in Table 6. $\dot{E}_f$, $\dot{E}_p$and $\dot{E}_d$ of each component in the proposed DWDOAS system with mode II and mode III may be derived similarly, only differing in the inlet air state and outlet air state of the wet membrane humidifier.

2.5. Economic analysis

The life cycle cost (*LCC*) and payback period (*PBP*) of the reference vapour compression refrigeration system and the proposed DWDOAS system were calculated to determine the feasibility of the proposed system in this study. *LCC* is the summation of the initial cost (*IC*) and operating cost (*OC*) throughout the lifecycle of the reference system and the proposed system. The present value method was used to calculate the *LCC*. The interest rate (i) and discount rate (d) are 4% and 3%, respectively (Abdel-Salam and Simonson, 2014). The useful life (n) is 15 years, and it is assumed that there were no residual values (Li et al., 2010).

Table 6
The fuel exergy rate, production exergy rate and destruction exergy of each component in the proposed DWDOAS system.

Component	Fuel exergy rate ($\dot{E}_f$)	Production exergy rate ($\dot{E}_p$)	Destruction exergy ($\dot{E}_d$)
DW	$\dot{E}_{DW} + \dot{E}_F - \dot{E}_E$	$\dot{E}_B - \dot{E}_A$	$\dot{E}_{DW} + \dot{E}_F - \dot{E}_E - (\dot{E}_B - \dot{E}_A)$
HP	$\dot{E}_D - \dot{E}_R$	$\dot{E}_C - \dot{E}_B$	$\dot{E}_D - \dot{E}_R - (\dot{E}_C - \dot{E}_B)$
WMH	$\dot{E}_{WMH} + \dot{E}_C$	$\dot{E}_{C'}$	$\dot{E}_{WMH} + \dot{E}_C - \dot{E}_{C'}$
AH	$\dot{E}_{AH} + \dot{E}_D$	$\dot{E}_E$	$\dot{E}_{AH} + \dot{E}_D - \dot{E}_E$
PF	$\dot{E}_{PF}$	$\dot{E}_S - \dot{E}_{C'}$	$\dot{E}_{PF} - (\dot{E}_S - \dot{E}_{C'})$
RF	$\dot{E}_{RF}$	$\dot{E}_G - \dot{E}_F$	$\dot{E}_{RF} - (\dot{E}_G - \dot{E}_F)$

2.6. Thermoeconomic analysis

Thermoeconomics is based on exergy analysis and economic principles. The cost rate balance for the kth component of the system based on the exergy rate and cost per unit exergy is defined as follows (Bejan et al., 1996):

$$\sum_e (c_e \dot{E}_e)_k + (c_w \dot{W})_k = (c_q \dot{E}_q)_k + \sum_i (c_i \dot{E}_i)_k + \dot{Z}_k \quad (5)$$

or

$$\sum_e \dot{C}_{e,k} + \dot{C}_{w,k} = \dot{C}_{q,k} + \sum_i \dot{C}_{i,k} + \dot{Z}_k \quad (6)$$

The capital cost rate ($\dot{Z}_k$) for the kth component of the system is defined as (Bejan et al., 1996):

$$\dot{Z}_k = \frac{Z_k \emptyset}{3600N} CRF \quad (7)$$

The capital recovery factor (*CRF*) is defined as (Bejan et al., 1996):

$$CRF = \frac{i(1+i)^n}{(1+i)^n - 1} \quad (8)$$

Based on Eqs. (5) and (6), exergetic cost rate balances and corresponding auxiliary equations for the components in the DWDOAS are presented in Table 7.

3. Performance indicators

3.1. Thermodynamic performance indicators

The thermodynamic performance of the DWDOAS can be assessed according to three aspects: the dehumidification performance, which consists of the moisture removal capacity (*MRC*) and the dehumidification rate on the process side (D_{sys}); the sensible heat performance, which consists of the sensible heat capacity (*SHC*) and the sensible heat efficiency on the process side (*SHE*); the regeneration performance, which consists of the regeneration heat capacity (*RHC*) and the thermodynamic coefficient on the regenerating side (*TCOP*).

3.1.1. Moisture removal capacity (MRC)

MRC_{DW} is the rate of moisture removed by the DW and is defined as:

$$MRC_{DW} = \dot{M}_{pro}(\omega_{DW,in} - \omega_{DW,out}) \quad (9)$$

MRC_{WMH} is the increased moisture content of air through the WMH and is defined as:

$$MRC_{WMH} = \dot{M}_{pro}(\omega_{WMH,in} - \omega_{WMH,out}) \quad (10)$$

MRC_{sys} is the change value of moisture removal of the DWDOAS and is defined as:

$$MRC_{sys} = \dot{M}_{pro}(\omega_{sys,in} - \omega_{sys,out}) \quad (11)$$

Table 7
Exergetic cost rate balances and corresponding auxiliary equation for the components in the DWDOAS.

Component	Cost rate balance	Auxiliary equations
PF	$\dot{Z}_F + \dot{C}_F = \dot{C}_S - \dot{C}_{C'}$	$\dot{C}_S = \dot{C}_{C'}$
RF	$\dot{Z}_R + \dot{C}_R = \dot{C}_F - \dot{C}_G$	$\dot{C}_F = \dot{C}_G$
DW	$\dot{Z}_{DW} + \dot{C}_{DW} + (\dot{C}_E - \dot{C}_F) = \dot{C}_B - \dot{C}_A$	$\dot{C}_A = 0$
HP	$\dot{Z}_{HP} + (\dot{C}_D - \dot{C}_{R'}) = \dot{C}_C - \dot{C}_B$	$\dot{C}_{R'} = 0$
WMH	$\dot{Z}_{WMH} + \dot{C}_{WMH} + \dot{C}_C = \dot{C}_{c'}$	-
AH	$\dot{Z}_{AH} + \dot{C}_{AH} + \dot{C}_D = \dot{C}_E$	-

3.1.2. Dehumidification rate (D_{sys})

D_{sys} is the rate of change in the air's moisture content after passing through the DWDOAS and is defined as:

$$D_{sys} = \frac{\omega_{sys,in} - \omega_{sys,out}}{\omega_{sys,in}} \tag{12}$$

3.1.3. Sensible heat capacity (SHC) on the process side

The inlet air of the DW on the process side is heated due to the adsorption heat that is generated when the adsorbent of the DW adsorbs water vapour. SHC_{DW} is the sensible heat capacity of the DW on the process side and is defined as:

$$SHC_{DW} = c_{pro}\dot{M}_{pro}\left(T_{dw,in} - T_{dw,out}\right) \tag{13}$$

The inlet air of the HP on the process side is cooled since the working fluid absorbs heat in the evaporator section of the HP. SHC_{HP} is the sensible heat capacity by HP on the process side and is defined as:

$$SHC_{HP} = c_{pro}\dot{M}_{pro}\left(T_{HP,in} - T_{HP,out}\right) \tag{14}$$

The inlet air of the WMH is cooled via heat and moisture exchange on the wet membrane surface of the WMH. SHC_{WMH} is the sensible heat capacity by WMH and is defined as:

$$SHC_{WMH} = c_{pro}\dot{M}_{pro}\left(T_{WMH,in} - T_{WMH,out}\right) \tag{15}$$

The process air of the DWDOAS on the process side is cooled due to the influences of the DW, HP and WMH. SHC_{sys} is the sensible heat capacity of the DWDOAS on the process side and is defined as:

$$SHC_{sys} = c_{pro}\dot{M}_{pro}\left(T_{sys,in} - T_{sys,out}\right) \tag{16}$$

3.1.4. Sensible heat efficiency (SHE) on the process side

SHE is the efficiency of temperature reduction of the DWDOAS and is defined as:

$$SHE = \frac{T_{sys,in} - T_{sys,out}}{T_{sys,in}} \tag{17}$$

3.1.5. Regeneration heat capacity (RHC) on the regenerating side

The regeneration heat is provided by the HP and air heater (AH). The inlet air of the HP on the regeneration side is heated since the working fluid releases heat in the condenser section of the HP. RHC_{HP} is the regeneration heat capacity of the HP on the regenerating side and is defined as:

$$RHC_{HP} = c_{reg}\dot{M}_{reg}\left(T_{HP,out} - T_{HP,in}\right) \tag{18}$$

RHC_{AH} is the regeneration heat capacity by the AH on the regenerating side and is defined as:

$$RHC_{AH} = c_{reg}\dot{M}_{reg}\left(T_{AH,out} - T_{AH,in}\right) \tag{19}$$

3.1.6. Thermodynamic coefficient (TCOP)

TCOP is the ratio between the refrigeration capacity of DWDOAS gained by the process air and the regenerating heating capacity and is defined as:

$$TCOP = \frac{\dot{M}_{pro}\left(h_{sys,in} - h_{sys,out}\right)}{c_{reg}\dot{M}_{reg}\left(T_{AH,out} - T_{AH,in}\right)} \tag{20}$$

3.2. Exergy performance indicators

The exergy efficiency of DWDOAS is the ratio of the production exergy rate E_p to the fuel exergy rate E_f and is defined as (Ge and Wang, 2020):

$$\eta = \frac{\dot{E}_P}{\dot{E}_f} = 1 - \frac{\dot{E}_d}{\dot{E}_f} \tag{21}$$

The destruction exergy ratio is defined as:

$$y_{d,k} = \frac{\dot{E}_{d,k}}{\dot{E}_f} \tag{22}$$

3.3. Economic performance indicators

Life cycle cost (*LCC*) and payback period (*PBP*) were selected as economic performance indicators in this study. The *LCC* and *PBP* are defined as (Duffie and Beckman, 2013):

$$LCC = IC + PWF{\cdot}OC \tag{23}$$

$$PWF = \begin{cases} \frac{1}{d-i}\left[1 - \left(\frac{1+i}{1+d}\right)^n \right. & if\ (i \neq d) \\ \frac{N}{N+1} & if\ (i = d) \end{cases} \tag{24}$$

$$PBP = \frac{IC_{prop} - IC_{conv}}{OC_{conv} - OC_{prop}} \tag{25}$$

3.4. Thermoeconomic performance indicators

The exergoeconomic factor expresses the relative significance of a component. The exergoeconomic factor is the ratio of the contribution from non-exergy-related cost to the total cost increase with the components of the system and is defined as (Mosaffa and Farshi, 2016):

$$f_k = \frac{\dot{Z}_k}{\dot{Z}_k + c_{f,k}\dot{E}_{D,K}} \tag{26}$$

4. Data acquisition and uncertainty

The system was instrumented to collect air temperatures, air humidity and air flow velocity. The locations of these instruments are shown in Fig. 1. The detailed parameters of the measured instruments are listed in Table 8. The measurements were evaluated with uncertainty analysis Arat et al., 2021). The uncertainties in the measurement of temperature, relative humidity and flow rate are ±0.09 ℃, ±1.5% and ±0.12 m/s, respectively. The error propagation for the performance indicators was calculated according to Eqs. (27) and ((28):

$$\Delta y = \left[\left(\frac{\partial f}{\partial x}\right)^2 (\Delta x_1)^2 + \left(\frac{\partial f}{\partial x_2}\right)^2 (\Delta x_2)^2 \cdots + \left(\frac{\partial f}{\partial x_n}\right)^2 (\Delta x_n)^2\right]^{\frac{1}{2}} \tag{27}$$

$$\frac{\Delta y}{y} = \left[\left(\frac{\partial f}{\partial x_1}\right)^2 \left(\frac{\Delta x_1}{y}\right)^2 + \left(\frac{\partial f}{\partial x_2}\right)^2 \left(\frac{\Delta x_2}{y}\right)^2 \cdots \left(\frac{\partial f}{\partial x}\right)^2 \left(\frac{\Delta x_n}{y}\right)^2\right]^{\frac{1}{2}} \tag{28}$$

where x_i is the independent variable, Δx_i is the absolute uncertainty associated with the variable x_i, y is the dependent variable, Δy is its absolute uncertainty, and f is a function of the independent variable x_i.

The results of the minimum and maximum relative uncertainty values obtained for the calculated parameters are as follows: ±5.0% for

Table 8
Measured parameters.

Measured parameter	Technical Properties	Measurement range	Accuracy
Temperature	PT 100	-40 ℃~100 ℃	±0.15 ℃
Relative humidity	Capacitive	0%~100%	±2%
Air velocity	Hot wire	0 m/s~10 m/s	±0.2 m/s

MRC_{DW}, ±5.1% for MRC_{WMH}, ±9.3% for SHC_{DW}, ±8.6% for SHC_{HP}, ±9.4% for SHC_{WMH}, ±9.7% for *SHE*, ±3.4% for RHC_{HP}, ±7.1% for RHC_{AH}, ±6.7% for D_{sys}, ±2.3% for *TCOP* and ±6.4% for η.

5. Results and discussion

5.1. Air conditioning system comparison

Using the above experimental setup, the thermal characteristics of the DWDOAS with the above three modes under the selected standard conditions (T_A: 32 ℃; ω_A: 18 g kg^{-1}; M_{pro}: 0.2 m^3 s^{-1}) were experimentally studied, and the changes in temperature, humidity and *TCOP* of the DWDOAS under different regeneration temperatures were evaluated to obtain the most suitable DOAS for a nZEB.

Table 9 shows the experimental results for three DWDOAS modes at a regeneration temperature of 80 ℃. Fig. 3 is the psychrometric chart of the three modes at a regeneration temperature of 80 ℃. The supply air state points (S) are shown in Fig. 3, in which the green area meets the requirements for air temperature and humidity of a nZEB (*T* is less than 26 ℃, and ω is less than 12.6 g kg^{-1}) (Lin et al., 2020).

As shown in Table 9 and Fig. 3, both mode I and mode III can meet the requirements of the supply air temperature T_S and ω_S humidity ratio for a nZEB, but the supply air temperature T_S of mode II reached 30.7 ℃. This result is because although the WMH placed upstream the condensing section of the HP can enhance the heat exchange efficiency of the HP by precooling the regenerative air to increase the temperature drop in the HP evaporation section, the heat transfer effect of HP is limited, and it is not enough to meet the temperature and humidity requirements of a nZEB. Therefore, only two modes of DWDOAS (mode I and mode III) that have WMHs downstream of the HP evaporation section can meet the requirements for supply air temperature and humidity.

The *TCOP* values of mode I and mode III at different regeneration temperatures were studied to further compare their performances. As shown in Fig. 4, the *TCOP* values of mode I and mode III decreased with increasing regeneration temperature, and mode III was always lower than mode I. The reason is that although the cooling capacity of the evaporation section of the HP increases by placing the wet membrane humidifier on the regeneration side, it also reduces the inlet temperature of the condensation section of the HP on the regeneration side, which increases the regeneration energy consumption.

Based on the fuel exergy rate, production exergy rate and destruction exergy of each component in the proposed system with the above three modes under the standard conditions (base value, see Table 5), the exergy performance of each component and the overall DWDOAS system can be obtained and summarized in Table 10.

As shown in Table 10, the exergy efficiency of mode I is the highest, followed by mode III and mode II. The exergy analyses reveal that the DW has the greatest destruction exergy. The major reason for the destruction exergy of the DW depends on the mixing of process and regeneration air and mass and heat transfer between the air and the desiccant matrix (Van den Bulck et al., 1988). AH is the second destruction exergy ratio. The sum of the DW and AH destruction exergy ratios reached 74.5% overall. Therefore, further efforts should be made to reduce the destruction exergy of the DW and AH.

Mode I has a greater thermodynamic coefficient and exergy efficiency than mode II and mode III. Thus, mode I is recommended for use as a DOAS for nZEBs.

5.2. The effect of the operating parameters

The main operating parameters for the thermodynamic and exergy performance of mode I, which are the process air inlet temperature, the process air inlet humidity ratio and the regeneration temperature, were studied.

5.2.1. Process air inlet temperature

The influence of the process air inlet temperature on the dehumidification performance, sensible heat performance, regeneration performance and exergy efficiency of the DWDOAS are studied as the T_A changed from 28 ℃ to 38 ℃, during which ω_A was 18 g kg^{-1}, M_{pro} was 0.2 m^3 s^{-1}, and T_{AH} was 80 ℃.

Fig. 5 shows that the latent heat of the DW was positive, thus dehumidifying the air, while that of the WMH was negative, thus humidifying the air. The moisture removal of the DW was much greater than that of the WMH. The dehumidification of DW decreased, the humidification of WMH increased, and D_{sys} decreased when T_A increased. The reason for the dehumidification decrease for DW is that the surface temperature of the adsorption material of the DW increases with an increasing T_A, which leads to an increase in the water vapour partial pressure on the surface of the adsorption material and a decrease in the mass transfer driving potential difference (Angrisani et al., 2012). The increase in the humidification of the WMH occurs because the mass transfer driving force of the WMH strengthens, which is due to the significant increase in the air inlet temperature. Combined with the dehumidification and humidification effects of the DW and WMH, the total moisture removal of the DWDOAS decreased from 1.11 g s^{-1} to 0.95 g s^{-1}, a decrease of 14.3%. D_{sys} also correspondingly decreased from 0.31 to 0.26.

Fig. 6 shows that the sensible heat capacity of the DW was negative, thus heating the air, while the sensible cooling capacities of the HP and WMH were positive, thus cooling the air. The sensible heat capacity of the DW decreased, the sensible cooling capacity of the HP and WMH increased, and *SHE* increased when T_A increased. The reason for the decrease in the sensible heat capacity of the DW is that the decrease in the moisture removal of DW leads to a decrease in the adsorption heat of the DW (Chen et al., 2018). The gradual increase in the sensible cooling capacity of the HP may be due to the increasing temperature difference between the evaporator section and the condenser section of the HP (Jung and Boo, 2014). The reason for the increase in the sensible cooling capacity of the WMH is that the increase in the inlet temperature enhances the heat transfer driving force of the WMH. Considering the combined effect of the three devices, the sensible cooling capacity of the DWDOAS increased with an increase in T_A, from 0.96 kW to 2.76 kW, an

Table 9
Experimental results for three DWDOAS modes at a regeneration temperature of 80 ℃.

State point	Mode I			Mode II			Mode III		
	t (℃)	ω (g kg^{-1})	RH (%)	t (℃)	ω (g kg^{-1})	RH (%)	t (℃)	ω (g kg^{-1})	RH (%)
A	32.0	18.0	60.2	32.0	18.0	60.2	32.0	18.0	60.2
B	46.5	11.6	16.4	46.5	11.6	16.4	46.5	11.6	16.4
C	33.2	11.6	35.3	30.7	11.6	39.7	30.7	11.6	39.7
S	23.5	12.7	69.0	30.7	11.6	39.7	22.5	12.8	73.8
R	25.0	8.8	43.8	25.0	8.8	43.8	25.0	8.8	43.8
R’	25.0	8.8	43.8	19.5	10.0	69.8	19.5	10.0	69.8
D	42.7	8.8	17.3	40.6	10.0	20.1	40.6	10.0	20.1
E	80.0	8.8	1.6	80.0	10.0	1.8	80.0	10.0	1.8
F	39.4	28.0	59.3	39.5	28.0	59.0	39.5	28.0	59.0

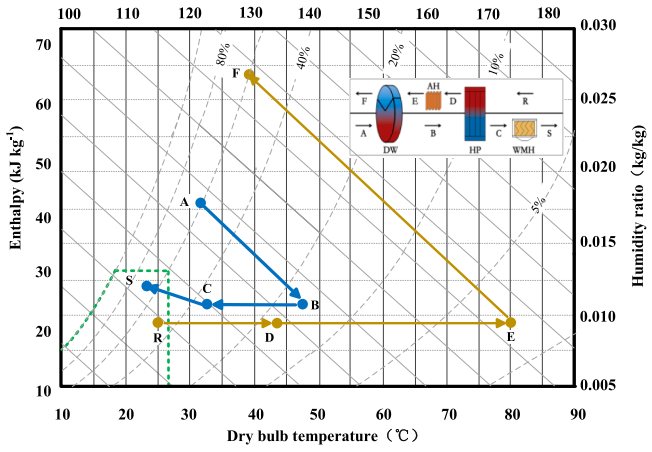

(a) Mode Ⅰ

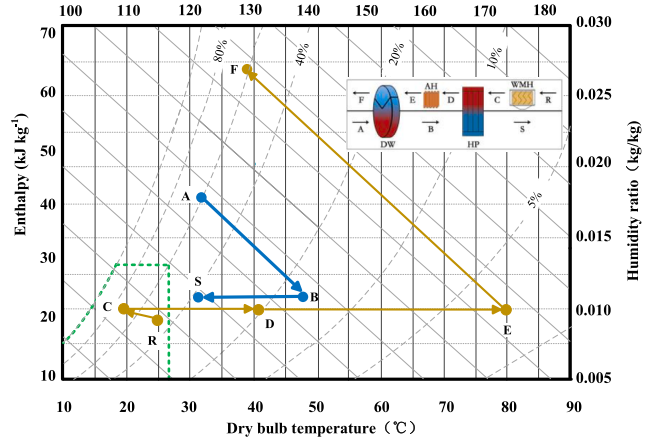

(b) Mode Ⅱ

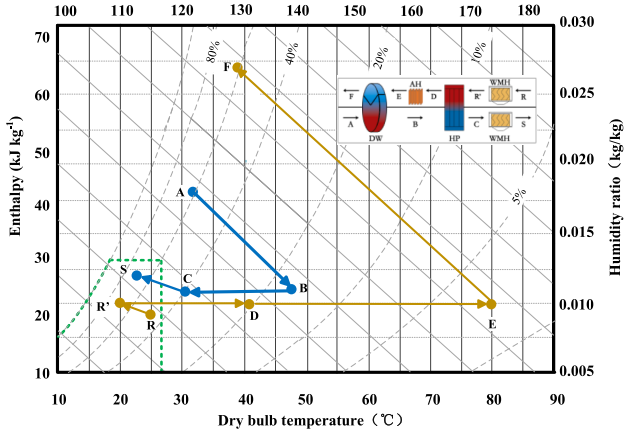

(c) Mode Ⅲ

Fig. 3. Process and regeneration of DWDOAS. (for T_A: 32 ℃; ω_A: 18 g kg^{-1}; M_{pro}: 0.2 m^3 s^{-1}; T_{AH}: 80 ℃).

increase of 187.5%, and the *SHE* also increased from 0.17 to 0.36.

Fig. 7 shows that RHC_{AH} and η decreased and RHC_{HP} and *TCOP* increased when T_A increased. The increase in RHC_{HP} is due to the significant increase in the inlet air temperature of the evaporator section of the HP on the process side, which enhances the heat transfer

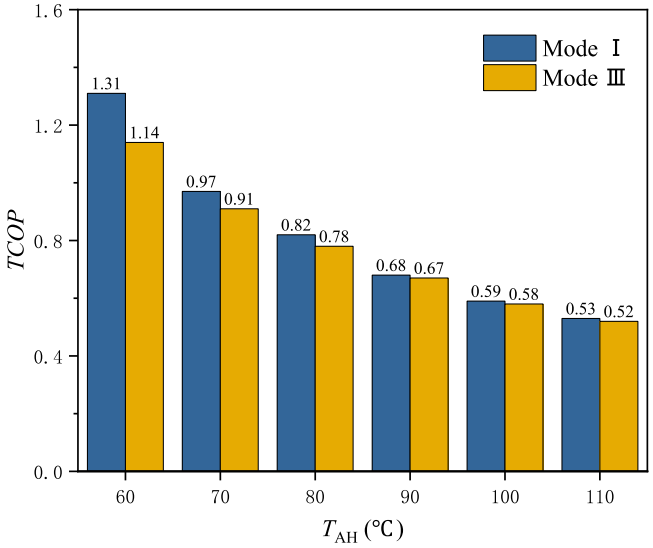

Fig. 4. *TCOP* values of mode I and mode III at different regeneration temperatures.

temperature difference of the HP. RHC_{AH} decreases when RHC_{HP} increases since the regeneration temperature required by the DW is designed as a fixed value and the total *RHC* of the DWDOAS remains unchanged. RHC_{HP} accounted for 31.4% to 33.6% of the total regeneration energy consumption. The *TCOP* increases because the cooling capacity increases and the regenerative heat capacity decreases. Therefore, the DWDOAS had a high performance coefficient in the high-temperature region. Increasing the process air inlet temperatures led to a decrease in the overall exergy efficiency of the DWDOAS system. The exergy efficiency trend shows that the production exergy rate increases as the refrigeration capacity increases, while the fuel exergy rate increases even more; thus, the exergy efficiency decreases.

5.2.2. *Process air inlet humidity ratio*

The influence of the process air inlet humidity ratio on the dehumidification performance, sensible heat performance, regeneration performance and exergy efficiency of the DWDOAS were studied as ω_A changed from 14 g/kg to 22 g/kg, during which T_A was 32 ℃, M_{pro} was 0.2 m^3 s^{-1}, and T_{AH} was 80 ℃.

Fig. 8 shows that the dehumidification of DW increased, the humidification of WMH decreased, and D_{sys} increased when ω_A increased. The dehumidification capacity increases with DW mainly because the high humidity results in greater desiccant wheel effectiveness due to the greater driving force of the mass transfer. The decrease in the humidification capacity of the WMH increases the process air inlet humidity ratio, which then increases the wet-bulb temperature of the process air entering the WMH. Combined with the dehumidification and humidification effects of the DW and WMH, the total moisture removal of the DWDOAS increased from 0.51 g s^{-1} to 1.51 g s^{-1}, an increase of 195%, and D_{sys} increased from 0.18 to 0.34.

Fig. 9 shows that the sensible heat capacity of DW increased, the sensible cool capacity of HP increased, the sensible cooling capacity of WMH decreased, and the *SHE* increased when ω_A increased. The reason for the increase in the sensible heat capacity of DW is that the increase in moisture removal leads to an increase in the adsorption heat of the DW. The reason why the sensible cooling capacity of HP increases slowly is that the heat transfer effect of the HP is not obvious due to the constant temperature of the condensing section. The reason for the decrease in the sensible cooling capacity of the WMH is that the increase in the inlet air wet-bulb temperature of the WMH inhibits the heat transfer driving force of the WMH. Considering the three devices, the sensible cooling capacity of the DWDOAS decreased with an increase in ω_A,-from 2.04

Table 10
The results of exergy analysis of the DWDOAS system.

Component	Mode I			Mode II			Mode III		
	$\dot{E}_d$	y_d	η	$\dot{E}_d$	y_d	η	$\dot{E}_d$	y_d	η
DW	0.68	52.4%	22.6%	0.64	48.6%	23.5%	0.64	46.8%	23.5%
HP	0.11	8.7%	87.2%	0.12	8.9%	86.7%	0.12	8.6%	86.5%
WMH (1)	0.04	3.1%	88.0%	-	-	-	0.05	3.8%	89.2%
WMH (2)	-	-	-	0.06	4.5%	91.8%	0.06	4.4%	91.8%
AH	0.29	22.1%	77.2%	0.32	24.4%	74.4%	0.32	23.3%	74.5%
PF	0.10	7.7%	80.2%	0.10	7.6%	80.4%	0.10	7.3%	80.6%
RF	0.08	6.0%	73.4%	0.08	6.0%	73.3%	0.08	5.8%	73.4%
DWDOAS	1.30	100%	43.3%	1.32	100%	40.3%	1.37	100%	41.4%

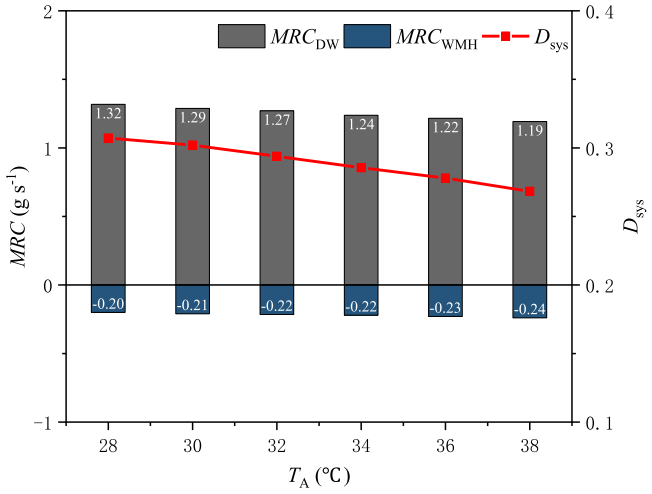

Fig. 5. Effect of T_A on the process side *MRC* and D_{sys} (for ω_A:18 g kg^{-1}; M_{pro}: 0.2 m^3 s^{-1}; T_{AH}: 80 ℃)

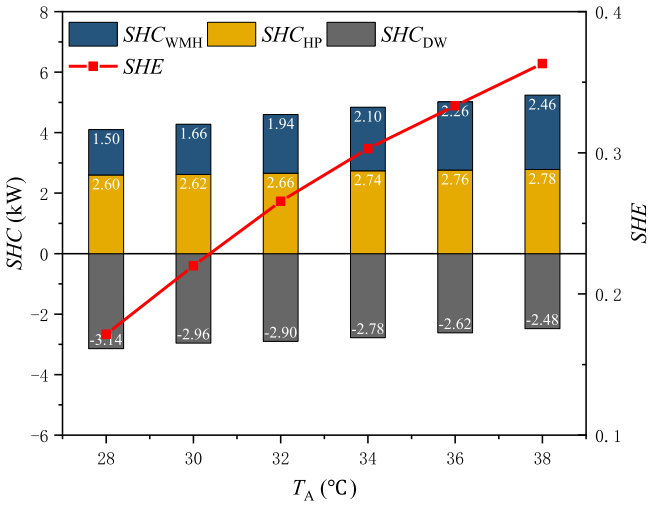

Fig. 6. Effect of T_A on the process side *SHC* and *SHE* (for ω_A:18 g kg^{-1}; M_{pro}: 0.2 m^3 s^{-1}; T_{AH}: 80 ℃).

kW to 1.28 kW, a decrease of 37.2%, and the *SHE* also decreased from 0.32 to 0.20.

Fig. 10 shows that RHC_{AH} and η decreased and RHC_{HP} and *TCOP* increased when ω_A increased. RHC_{HP} accounted for 28.9% to 34.7% of the total regeneration energy consumption. The *TCOP* value increases because the latent heat transfer of the DWDOAS increases greatly, which increases the cooling capacity. Therefore, the DWDOAS had a high performance coefficient in the high-humidity region, which is greatly beneficial to the energy savings of a DOAS in high-humidity regions. η

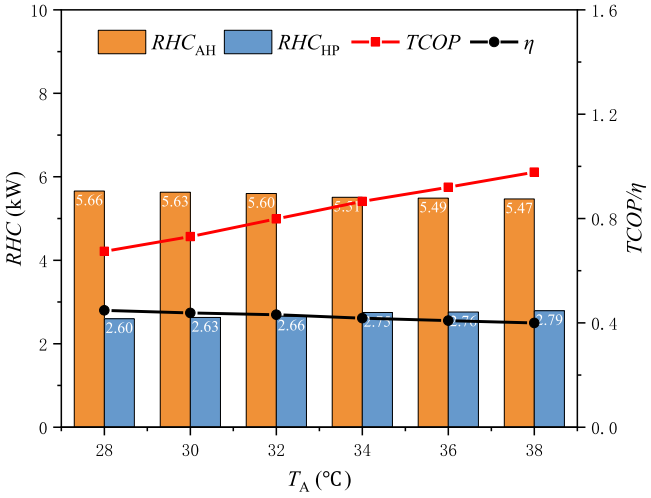

Fig. 7. Effect of T_A on the regeneration side *RHC* and *TCOP* (for ω_A: 18 g kg^{-1}; M_{pro}: 0.2 m^3 s^{-1}; T_{AH}: 80 ℃).

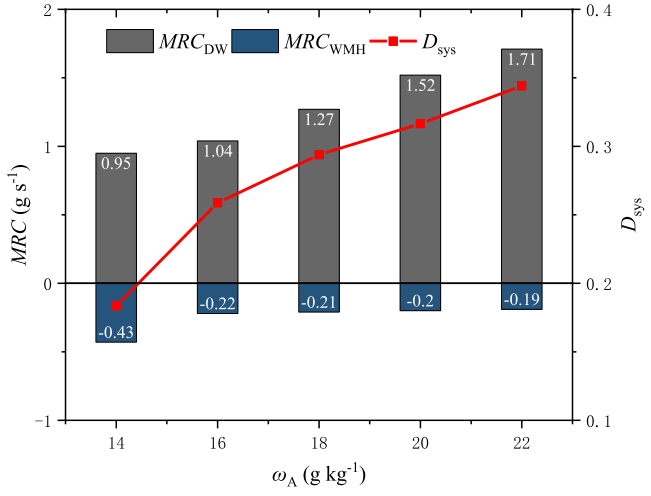

Fig. 8. Effect of ω_A on the process side *MRC* and D_{sys} (for T_A: 32℃; M_{pro}: 0.2 m^3 s^{-1}; T_{AH}: 80 ℃)

decreased when ω_A increased, suggesting that the increase in the production exergy rate with increasing ω_A is greater than the increase in the fuel exergy rate, which further increases the exergy efficiency.

5.2.3. *Regeneration temperature*

The influence of the regeneration temperature on the dehumidification performance, sensible heat performance, regeneration performance and exergy efficiency of DWDOAS were studied as the T_{AH} changed from 60 ℃ to 110 ℃, during which T_A was 32 ℃, ω_A was 18 g kg^{-1}, and M_{pro} was 0.2 m^3 s^{-1}.

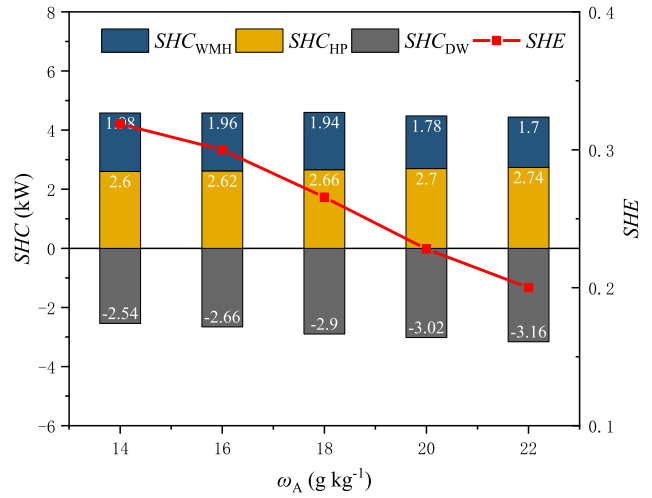

Fig. 9. Effect of ω_A on the process side *SHC* and *SHE* (for T_A: 32 ℃; M_{pro}: 0.2 m^3 s^{-1}; T_{AH}: 80 ℃)

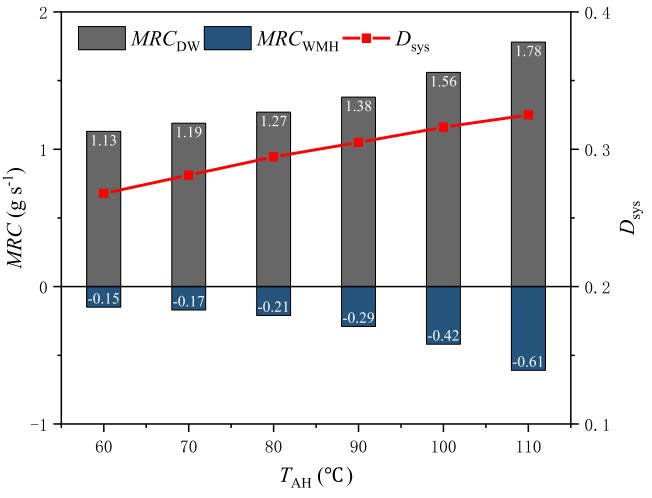

Fig. 11. Effect of T_{AH} on the process side *MRC* and D_{sys} (for T_A: 32 ℃; ω_A: 18 g kg^{-1}; M_{pro}: 0.2 m^3 s^{-1}).

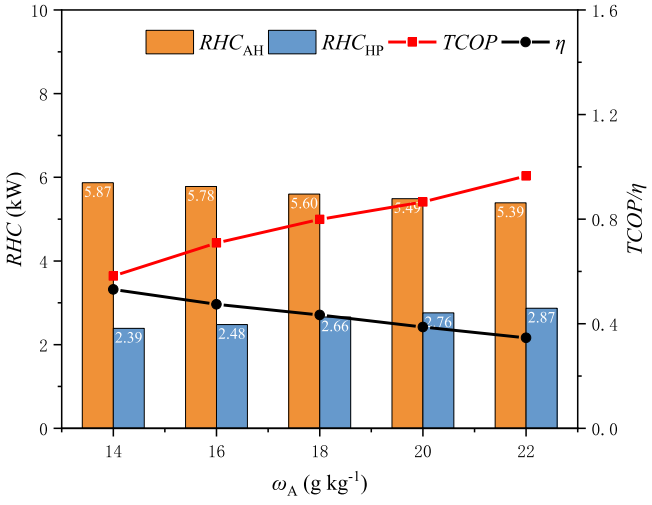

Fig. 10. Effect of ω_A on the regeneration side *RHC* and *TCOP* (for T_A: 32 ℃; M_{pro}:0.2 m^3 s^{-1}; T_{AH}:80 ℃).

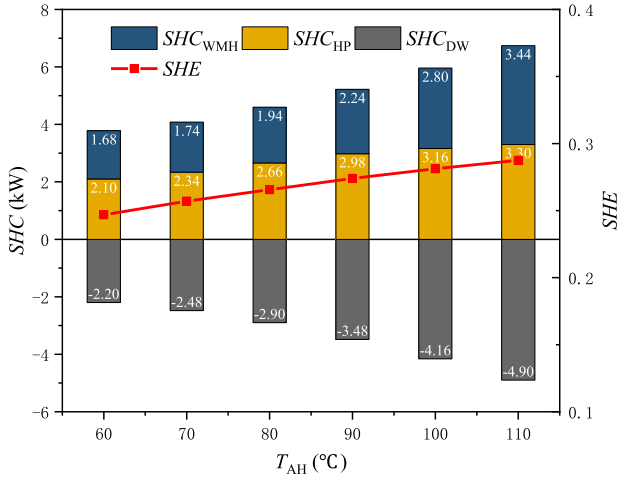

Fig. 12. Effect of T_{AH} on the process side *SHC* and *SHE* (for T_A: 32 ℃; ω_A: 18 g kg^{-1}; M_{pro}: 0.2 m^3 s^{-1}).

Fig. 11 shows that the dehumidification of DW increased, the humidification of WMH increased, and D_{sys} increased when T_{AH} increased. The reason for the increase in the DW dehumidification capacity is that more water vapour is desorbed on the regeneration side, which means that the adsorbent can absorb more moisture on the DW process side with an increase in T_{AH}. An increased T_{AH} can improve the *MRC*, but it increases the temperature of the supply air. Lowering the wet-bulb temperature of the process air entering the WMH enhances the mass transfer of the WMH; therefore, the humidification of the WMH increased, and D_{sys} increased from 0.27 to 0.33.

Fig. 12 shows that the sensible heat capacity of DW increased, the sensible cooling capacity of HP and WMH increased, and *SHE* decreased when T_{AH} increased. The reason for the increase in the sensible heat capacity of DW is that the increase in the dehumidification of DW generates more adsorption heat. Considering the three devices, the sensible cooling capacity of the DWDOAS increased with an increase in T_{AH}, from 1.58 kW to 1.84 kW, an increase of 16.5%, and the *SHE* increased from 0.25 to 0.29.

Fig. 13 shows that RHC_{AH} and RHC_{HP} increased and *TCOP* and η decreased when T_{AH} increased. RHC_{HP} accounts for 26% to 40% of the total regeneration energy consumption. The energy consumption of AH increased significantly with increasing T_{AH}. Although the heat capacity

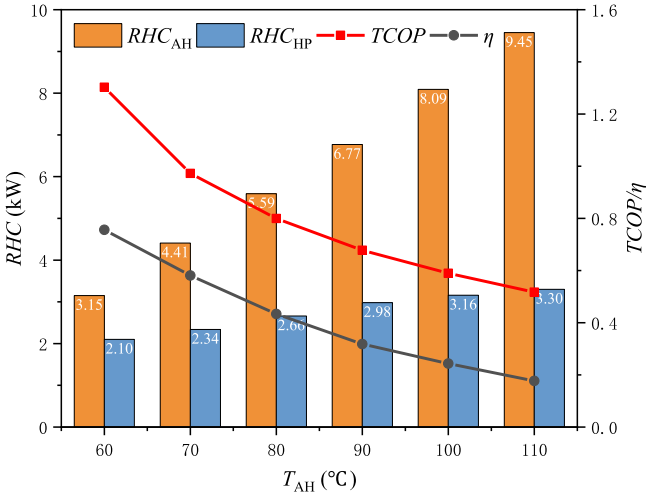

Fig. 13. Effect of T_{AH} on the regeneration side *RHC* and *TCOP* (for T_A: 32 ℃; ω_A: 18 g kg^{-1}; M_{pro}: 0.2 m^3 s^{-1}).

of the condenser side of the HP also increased, the increase was much less than that of the regeneration temperature; thus, RHC_{AH} increased, and *TCOP* decreased from 1.3 to 0.52. The η trend was similar to *TCOP*. This finding is due to the increase in irreversibility of the air heater (Van den Bulck et al., 1988).

5.3. Economic performance

5.3.1. Economic comparison between conventional and proposed DWDOAS systems

An economic comparison between the conventional and proposed DWDOAS systems is presented and discussed. The refrigeration capacity of the conventional and proposed DWDOAS systems was 50 kW. The total capital investments are provided based on the manufacturers and the literature. According to the different regenerative heat sources, two kinds of proposed DWDOAS systems were studied. One was a DWDOAS with a solar heater, and the other was a DWDOAS with an electric heater.

The system operation time is 1200 h. The price of electricity is \$0.12/kWh. The *IC* of the DW is \$6000/(m^3/s). The *IC* of air heater, heat pipe heat exchanger and electric heater are estimated to be \$7062/(m^3/s), \$350/m^2 and \$45/kW, respectively (Abdel-Salam and Simonson, 2014, Kim and Zhang, 2018). The *IC* of the WMH is \$50/kW (Baakeem et al., 2018). The *IC* of the tank, pump and fan are assumed to cost \$134.2/m^3, \$1.7/W and \$851/(m^3/s), respectively (Abdel-Salam and Simonson, 2014, Zhang et al., 2018). The *IC* of the solar collector is \$128.3/m^2 (Sonsaree et al., 2017). The *IC* of the conventional systems (direct expansion chiller) is \$171/kW.

Table 11 shows the *IC, OC, LCC* and *PBP* for comparison between the conventional and proposed DWDOAS systems. Although the *IC* of the proposed air conditioning system was higher, the *OC* was significantly lower than that of conventional air conditioning, in which the operating cost of a DWDOAS with an electric heater was reduced by 46% and that of a DWDOAS with a solar heater was reduced by 66%. The *LCCs* of the DWDOAS with an electric heater and the DWDOAS with a solar heater were reduced by 21% and 30%, respectively, and the payback periods were 6.8 years and 5.7 years, respectively, which indicates the proposed DWDOAS with a solar heater achieves competitive economic performance. The reason why the operating cost of a DWDOAS is greatly reduced is that the additional energy required to the system is low because the HP does not need additional energy and the WMH consumes less energy. The main energy consumption of the system is generated from the heater. When the solar thermal system is used, the consumption of the heater is reduced accordingly.

5.3.2. Thermoeconomical analysis

A thermoeconomical analysis of the proposed DWDOAS systems under standard conditions was conducted. The results for all the DWDOAS components are illustrated in Table 12. The f reflects the proportion of the non-exergy cost in the total cost of the system. When f is low and the exergy efficiency is also low, it can be considered to replace the component with a more efficient and expensive component. Conversely, when f is high and exergy efficiency is also high, components with low efficiency and low price can be used (Abdel-Salam and Simonson, 2014). The relatively large value of f and η (see Table 10) for the HP suggests that the investment costs of the HP should be lowered. The large value of f and smaller value of η (see Table 10) for the DW suggests that the investment costs of the DW should be lowered and the efficiency of the DW should be improved.

6. Conclusion

A dedicated desiccant wheel outdoor air cooling system (DWDOAS) suitable for nZEBs in high-temperature and high-humidity areas was proposed. The energy, exergy and economic performance of DWDOAS were investigated through experiments. Additionally, the main operating parameters affecting DWDOAS performance were investigated through experiments. According to the analysis, several conclusions were drawn.

Table 11
Economic performance comparison of the conventional and proposed DWDOAS systems.

	Conventional systems	DWDOAS with solar heater	DWDOAS with electric heater
IC (\$)	12405	24329	21797
OC (\$)	3024	1016	1639
LCC (\$)	59579	41473	47365
PBP (year)	-	5.7	6.8

Table 12
The results of thermoeconomical analysis for the proposed DWDOAS systems.

Component	DW	HP	WMH	AH	PF	RF
f	86.6%	78.0%	32.6%	39.9%	53.7%	34.6%

a Three DWDOAS modes were proposed. The results show that mode I (WMH placed upstream of the HP evaporation section) and mode III (two WMHs placed upstream of the HP evaporation section and in front of the HP condensation section) can meet the requirements for supply air temperature and humidity. However, the thermodynamic coefficient *TCOP* and the exergy efficiency η of mode III were lower than those of mode I; therefore, mode I is recommended for nZEBs.

b The heat exchange capacity of the HP was evident during the experimental process, which not only significantly reduced the temperature of the air on the process side but also increased the temperature of the air on the regeneration side. RHC_{HP} accounted for 40% of the total regeneration energy consumption at most, which significantly reduced the regenerative energy consumption. In addition, HPs do not consume extra energy during operation, which increased the energy savings of the DWDOAS.

c The *TCOP* value decreased from 1.30 to 0.52, and the η value decreased from 0.76 to 0.18 when the regeneration temperature increased from 60 ℃ to 110 ℃. The regeneration temperature T_{AH} should be as low as possible to minimize energy consumption. DWDOAS driven by low-grade solar energy will further improve the performance coefficient of the DWDOAS in application.

d The life cycle cost of a DWDOAS with a solar heater was reduced by 30% compared to a conventional system and the payback period was 5.7 years, which indicates that the proposed DWDOAS with a solar heater achieves competitive economic performance.

Declaration of Competing Interest

None

Acknowledgements

This study was supported by the National Natural Science Foundation of China (Grant No. 51404191).

Please find the manuscript titled “Experimental investigation of dedicated desiccant wheel outdoor air cooling systems for nearly zero energy buildings”, which is submitted for possible publication in the International Journal of Refrigeration. This paper has not been published previously and is not under consideration for publication elsewhere. If accepted it will not be published elsewhere in the same form. The authors declare that there is no conflict of interests regarding the publication of this article.

Supplementary materials

Supplementary material associated with this article can be found, in the online version, at doi:10.1016/j.ijrefrig.2021.11.016.

References

Shu, H.W., Bie, X., Zhang, H.L., Xu, X.Y., Du, Y., Ma, Y., Duanmu, L., Cao, G.Y., 2020. Natural heat transfer air-conditioning terminal device and its system configuration for ultra-low energy buildings. Renewable Energy 154, 1113–1121. https://doi.org/10.1016/j.renene.2019.12.152.

Lopez-Ochoa, L.M., Las-Heras-Casas, J., Lopez-Gonzalez, L.M., Olasolo-Alonso, P., 2019. Towards nearly zero-energy buildings in Mediterranean countries: Energy Performance of Buildings Directive evolution and the energy rehabilitation challenge in the Spanish residential sector. Energy, 176, 335–352. https://doi.org/10.1016/j.energy.2019.03.122.

Li, Z.R., Zhang, D.K., Li, C., 2021. Experimental evaluation of indoor thermal environment with modularity radiant heating in low energy buildings. International Journal of Refrigeration 123, 159–168. https://doi.org/10.1016/j.ijrefrig.2020.11.018.

Papadopoulos, S., Kontokosta, C.E., Vlachokostas, A., Azar, E., 2019. Rethinking HVAC temperature setpoints in commercial buildings: The potential for zero-cost energy savings and comfort improvement in different climates. Building and Environment 155, 350–359. https://doi.org/10.1016/j.buildenv.2019.03.062.

Huang, H., Iman Binti Wan Mohd Nazi, W., Yu, Y., Wang, Y., 2020. Energy performance of a High-rise Residential Building Retrofitted to Passive Building Standard - A Case Study. Applied Thermal Engineering 181, 115902. https://doi.org/10.1016/j.applthermaleng.2020.115902.

Jahani, E., Cetin, K., Cho, I.H., 2020. City-scale single family residential building energy consumption prediction using genetic algorithm-based Numerical Moment Matching technique. Building and Environment 172, 106667. https://doi.org/10.1016/j.buildenv.2020.106667.

Liu, Z., Li, W., Chen, Y., Luo, Y., Zhang, L., 2018. Review of energy conservation technologies for fresh air supply in zero energy buildings. Applied Thermal Engineering 148, 544–556. https://doi.org/10.1016/j.applthermaleng.2018.11.085.

Chuah, Y.K., Yang, J.J., 2020. A integrated dedicated outdoor air system to optimize energy saving. Sustainability 12, 1051. https://doi.org/10.3390/su12031051.

Yang, S., Wan, M.P., Ng, F.B., Dubey, S., Henze, G.P., Chen, W., Baskaran, K., 2020. Experimental study of model predictive control for an air-conditioning system with dedicated outdoor air system. Applied Energy 257, 113920. https://doi.org/10.1016/j.apenergy.2019.113920.

S.Y. Cheon, H.J. Cho, J.W. Jeong. Energy saving potential of a vacuum-based membrane dehumidifier in a dedicated outdoor air system. Energy Conversion and Management, 227(2021)113618.https://doi.org/10.1016/j.enconman.2020.113618.

Tian, S.T., Su, X., Li, H., Huang, Y.X., 2021. Using a coupled heat pump desiccant wheel system to improve indoor humidity environment of nZEB in Shanghai: Analysis and optimization. Building and Environment 206, 109391. https://doi.org/10.1016/j.buildenv.2021.108391.

Jani, D.B., Mishra, M., Sahoo, P.K., 2018. A critical review on application of solar energy as renewable regeneration heat source in solid desiccant-vapor compression hybrid cooling system. Journal of Building Engineering 18, 107–124. https://doi.org/10.1016/j.jobe.2018.03.012.

Tang, W., Weng, Y., Zhang, Y., Cao, X., 2021. Path analysis of implementing carbon neutral target in customer side of power grid company. IOP Conference Series: Earth and Environmental Science 661, 12020. https://doi.org/10.1088/1755-1315/661/1/012020.

Jani, D.B., Mishra, M., Sahoo, P.K., 2016. Solid desiccant air conditioning-A state of the art review. Renewable & Sustainable Energy Reviews 60, 1451–1469. https://doi.org/10.1016/j.rser.2016.03.031.

Asadi, A., Meratizaman, M., Hosseinjani, A.A., 2020. Feasibility study of small-scale gas engine integrated with innovative net-zero water desiccant cooling system and single-effect thermal desalination unit. International Journal of Refrigeration 119, 276–293. https://doi.org/10.1016/j.ijrefrig.2020.06.025.

Ukai, M., Tanaka, H., Okumiya, M., 2018. Performance analysis and evaluation of desiccant air-handling unit under various operation condition through measurement and simulation in hot and humid climate. Energy and Buildings 172, 478–492. https://doi.org/10.1016/j.enbuild.2018.04.040.

Tu, R., Hwang, Y., 2018. Efficient configurations for desiccant wheel cooling systems using different heat sources for regeneration. International Journal of Refrigeration 86, 14–27. https://doi.org/10.1016/j.ijrefrig.2017.12.001.

Kubota, M., Hanada, T., Yabe, S., Matsuda, H., 2013. Regeneration characteristics of desiccant rotor with microwave and hot-air heating. Applied Thermal Engineering 50, 1576–1581. https://doi.org/10.1016/j.applthermaleng.2011.11.044.

Chaudhary, G.Q., Ali, M., Sheikh, N.A., Syed, I., Khushnood, S., 2018. Integration of solar assisted solid desiccant cooling system with efficient evaporative cooling technique for separate load handling. Applied Thermal Engineering 140, 696–706. https://doi.org/10.1016/j.applthermaleng.2018.05.081.

Heidari, A., Roshandel, R., Vakiloroaya, V., 2019. An innovative solar assisted desiccant-based evaporative cooling system for co-production of water and cooling in hot and humid climates. Energy Conversion and Management 185, 396–409. https://doi.org/10.1016/j.enconman.2019.02.015.

Chen, L., Tan, Y.K., 2020. The performance of a desiccant wheel air conditioning system with high-temperature chilled water from natural cold source. Renewable Energy 146, 2142–2157. https://doi.org/10.1016/j.renene.2019.08.082.

Yue, C., Zhang, Q., Zhai, Z., Ling, L., 2019. Numerical investigation on thermal characteristics and flow distribution of a parallel micro-channel separate heat pipe in data center. International Journal of Refrigeration 98, 150–160. https://doi.org/10.1016/j.ijrefrig.2018.10.025.

Milani, S.K., Ellahi, R., Mirzakhanlari, S., Mamourian, M., 2016. Enhancement of heat transfer and heat exchanger effectiveness in a double pipe heat exchanger filled with porous media: Numerical simulation and sensitivity analysis of turbulent fluid flow. Applied Thermal Engineering 109, 761–774. https://doi.org/10.1016/j.applthermaleng.2016.08.116.

Anand, R.S., Jawahar, C.P., Solomon, A.B., Bellos, E., 2020. A review of experimental studies on cylindrical two-phase closed thermosyphon using refrigerant for low-temperature applications. International Journal of Refrigeration 120, 296–313. https://doi.org/10.1016/j.ijrefrig.2020.08.011.

Qu, Y., Wang, S., Tian, Y., 2018. A review of thermal performance in multiple evaporators loop heat pipe. Applied Thermal Engineering 143, 209–224. https://doi.org/10.1016/j.applthermaleng.2018.07.070.

Wang, H., Zhou, S., Wei, Z., Wang, R., 2016. A study of secondary heat recovery efficiency of a heat pipe heat exchanger air conditioning system. Energy and Buildings 133, 206–216 https://doi.org/10.1016/j.enbuild.2016.09.061.

Monirimanesh, N., Nowee, S.M., Khayyami, S., Abrishamchi, I., 2016. Performance enhancement of an experimental air conditioning system by using TiO2/methanol nanofluid in heat pipe heat exchangers. Heat and Mass Transfer 52, 1025–1035. https://doi.org/10.1007/s00231-015-1615-2.

Chen, L., Chen, S., Liu, L., Zhang, B., 2018. Experimental investigation of precooling desiccant-wheel air-conditioning system in a high-temperature and high-humidity environment. International Journal of Refrigeration 95, 83–92. https://doi.org/10.1016/j.ijrefrig.2018.08.015.

Martinez, P.J., Martinez, P., Soto, V.M., Kaiser, A.S., 2018. Comparison of the performance of two different DOAS configurations involving conventional and renewable energies. Solar Energy 169, 284–296. https://doi.org/10.1016/j.solener.2018.05.002.

S. He, Z. Guan, H. Gurgenci, K. Hooman, Y. Lu, A.M. Alkhedhair. Experimental study of film media used for evaporative pre-cooling of air. Energy Conversion and Management, 87(2014) 874-884. https://doi.org/10.1016/j.enconman.2014.07.084.

A. Malli, H.R. Seyf, M. Layeghi, S. Sharifian, H. Behravesh. Investigating the performance of cellulosic evaporative cooling pads. Energy Conversion and Management, 52 (2011) 2598-2603. https://doi.org/10.1016/j.enconman.2010.12.015.

Kabeel, A.E., Bassuoni, M.M., 2017. A simplified experimentally tested theoretical model to reduce water consumption of a direct evaporative cooler for dry climates. International Journal of Refrigeration 82, 487–494. https://doi.org/10.1016/j.ijrefrig.2017.06.010.

Chiesa, G., Huberman, N., Pearlmutter, D., 2019. Geo-climatic potential of direct evaporative cooling in the mediterranean region: a comparison of key performance indicators. Building and Environment 151, 318–337. https://doi.org/10.1016/j.buildenv.2019.01.059.

Zhang, L., Liu, X., Jiang, Y., 2015. Exergy analysis of parameter unmatched characteristic in coupled heat and mass transfer between humid air and water. International Journal of Heat & Mass Transfer 84, 327–338. https://doi.org/10.1016/j.ijheatmasstransfer.2015.01.023.

Wang, L., Li, N.P., 2011. Exergy transfer and parametric study of counter flow wet cooling towers. Applied Thermal Engineering 31, 954–960. https://doi.org/10.1016/j.applthermaleng.2010.11.019.

Valero, A., Serra, L., Uche, J., 2006. Fundamentals of exergy cost accounting and thermoeconomics. Part I: theory. Journal of Energy Resources Technology 128, 1–8.

Abdel-Salam, A.H., Simonson, C.J., 2014. Annual evaluation of energy, environmental and economic performances of a membrane liquid desiccant air conditioning system with/without ERV. Applied Energy 116, 134–148. https://doi.org/10.1016/j.apenergy.2013.11.047.

Li, Y.T., Lu, L., Yang. Simonson, H.X., 2010. Energy and economic performance analysis of an open cycle solar desiccant dehumidification air-conditioning system for application in Hong Kong. Solar Energy 84, 2085–2095. https://doi.org/10.1016/j.solener.2010.09.006.

Bejan, A., Tsatsaronis, G., Moran, M., 1996. Thermal design and optimization. John Wiley & Sons, Inc, New York.

Ge, F.H., Wang, C., 2020. Exergy analysis of dehumidification systems: A comparison between the condensing dehumidification and the desiccant wheel dehumidification. Energy Conversion and Management 224, 113343. https://doi.org/10.1016/j.enconman.2020.113343.

Duffie, J.A., Beckman, W.A., 2013. Solar engineering of thermal processes. 4thed. John Wiley & Sons, Inc, New York.

Mosaffa, A.H., Farshi, L.G., 2016. Exergoeconomic and environmental analyses of an air conditioning system using thermal energy storage. Applied Energy 162, 515–526. https://doi.org/10.1016/j.apenergy.2015.10.122.

Arat, H., Arslan, O., Ercetin, U., Akbulut, A., 2021. Experimental study on heat transfer characteristics of closed thermosyphon at different volumes and inclination angles for variable vacuum pressures. Case Studies in Thermal Engineering 26, 101117. https://doi.org/10.1016/j.csite.2021.101117.

Lin, Y., Zhong, S., Yang, W., Hao, X., Li, C.Q., 2020. Towards Zero-Energy Buildings in China: A Systematic Literature Review. Journal of Cleaner Production 276, 123297. https://doi.org/10.1016/j.jclepro.2020.123297.

Van den Bulck, E., Klein, S.A., Mitchell, J.W., 1988. Second law analysis of solid desiccant rotary dehumidifiers. Journal of solar energy engineering-Transactions of the ASME 110, 2–9.

Angrisani, G., Minichiello, F., Roselli, C., Sasso, M., 2012. Experimental analysis on the dehumidification and thermal performance of a desiccant wheel. Applied Energy 92, 563–572. https://doi.org/10.1016/j.apenergy.2011.11.071.

Jung, E.G., Boo, J.H., 2014. Thermal analytical model of latent thermal storage with heat pipe heat exchanger for concentrated solar power. Solar Energy 10, 318–332 https://doi.org/10.1016/j.solener.2013.11.008.

Kim, Y., Zhang, Q., 2018. Economic and environmental life cycle assessments of solar water heaters applied to aquaculture in the US. Aquaculture 495, 44–54. https://doi.org/10.1016/j.aquaculture.2018.05.022.

Baakeem, S.S., Orfi, J., Bessadok-Jemai, A., 2018. Thermodynamic and economic analysis of the performance of a direct evaporative cooler working under extreme summer weather conditions. Journal of Mechanical Science and Technology 32, 1815–1825. https://doi.org/10.1007/s12206-018-0338-y.

Zhang, K., Zhao, D.L., Yin, X.B., Yang, R.G., Tan, G., 2018. Energy saving and economic analysis of a new hybrid radiative cooling system for single-family houses in the USA. Applied Energy 224, 371–381. https://doi.org/10.1016/j.apenergy.2018.04.115.

Sonsaree, S., Asaoka, T., Jiajitsawat, S., Aguirre, H., Tanaka, K., 2017. VCHP-ORC power generation from low-grade industrial waste heat combined with solar water heating system: Power generation and CO2 emission in industrial estate of Thailand. Cogent Engineering 4. https://doi.org/10.1080/23311916.2017.1359397, 1359397.